New Journal of Physics
The open access journal at the forefront of physics
Deutsche Physikalische Gesellschaft DPG IOP Institute of Physics

PAPER • OPEN ACCESS

Fermionic Hubbard model with Rashba or Dresselhaus spin–orbit coupling

To cite this article: Fadi Sun *et al* 2017 *New J. Phys.* **19** 063025

IOP Publishing New J. Phys. 19 (2017) 063025 https://doi.org/10.1088/1367-2630/aa6e31

New Journal of Physics

The open access journal at the forefront of physics

Deutsche Physikalische Gesellschaft DPG

IOP Institute of Physics

Published in partnership with: Deutsche Physikalische Gesellschaft and the Institute of Physics

CrossMark

OPEN ACCESS

RECEIVED
28 December 2016

REVISED
10 April 2017

ACCEPTED FOR PUBLICATION
20 April 2017

PUBLISHED
20 June 2017

PAPER

Fermionic Hubbard model with Rashba or Dresselhaus spin–orbit coupling

Fadi Sun[1,2,3,4], Jinwu Ye[1,3,4] and Wu-Ming Liu[2]

[1] Department of Physics, Capital Normal University, Key Laboratory of Terahertz Optoelectronics, Ministry of Education, and Beijing Advanced innovation Center for Imaging Technology, Beijing, 100048, People's Republic of China

[2] Beijing National Laboratory for Condensed Matter Physics, Institute of Physics, Chinese Academy of Sciences, Beijing 100190, People's Republic of China

[3] Department of Physics and Astronomy, Mississippi State University, MS 39762, United States of America

[4] Kavli Institute of Theoretical Physics, University of California, Santa Barbara, Santa Barbara, CA 93106, United States of America

E-mail: jy306@msstate.edu

Keywords: Rashba spin–orbit coupling, Hubbard interaction, incommennsurate magnons

Abstract

In this work, we investigate the possible dramatic effects of Rashba or Dresselhaus spin–orbit coupling (SOC) on the fermionic Hubbard model in a two-dimensional square lattice. In the strong coupling limit, it leads to the rotated antiferromagnetic Heisenberg model which is a new class of quantum spin model. For a special equivalent class, we identify a new spin–orbital entangled commensurate ground (Y-y) state subject to strong quantum fluctuations at $T = 0$. We evaluate the quantum fluctuations by the spin wave expansion up to order $1/S^2$. In some SOC parameter regimes, the Y-y state supports a massive relativistic incommensurate magnon (C-IC) with its two gap minima positions continuously tuned by the SOC parameters. The C-IC magnons dominate all the low temperature thermodynamic quantities and also lead to the separation of the peak positions between the longitudinal and the transverse spin structure factors. In the weak coupling limit, any weak repulsive interaction also leads to a weak Y-y state. There is only a crossover from the weak to the strong coupling. High temperature expansions of the specific heats in both weak and strong coupling are presented. The dramatic roles to be played by these C-IC magnons at generic SOC parameters or under various external probes are hinted at. Experimental applications to both layered noncentrosymmetric materials and cold atoms are discussed.

1. Introduction

It is well known that it is the strong electron correlations [1–6] which lead to many important phenomena such as antiferromagnetism, the spin density wave, charge density wave, putative spin liquids with topological orders, unconventional superconductivity, etc. Rashba or Dresselhaus spin–orbit coupling (SOC) [7] is ubiquitous in various two-dimensional (2D) or layered insulators, semiconductor systems, metals and superconductors without inversion symmetry [8–14]. Due to their tunability and controllability, strongly correlated Fermi gases on optical lattices have been attempted with some success to quantum simulate some of these phenomena [15, 16]. There are very recent notable experimental advances in generating 2D Rashba or Dresselhaus SOC or any of their linear combinations for cold atoms in both continuum and optical lattices [17–20]. It therefore becomes topical and important to investigate the combined effects of strong correlations and Rashba SOC in various lattice systems.

In this paper, we address this outstanding problem. Specifically, we investigate the system of interacting fermions at half filling hopping in a 2D square lattice subject to any combinations of Rashba or Dresselhaus SOC. In the strong coupling limit, we reach a novel quantum spin model named the rotated antiferromagnetic Heisenberg model (RAFHM) which is a new class of quantum spin model. For a special combination of Rashba

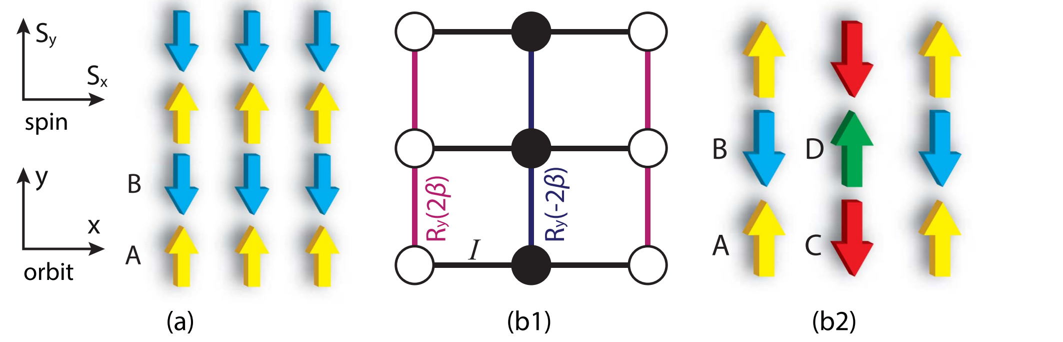

Figure 1. (a) The Y-y ground state in a square lattice in the original basis. One only needs to introduce two Holstein–Primakoff (HP) bosons corresponding to the A, B sublattice structure. (b1) The $(\pi, 0)$ sublattice structure of the Hamiltonian equation (2) in the $U(1)$ basis. (b2) The Y-(π, π) Néel state in the $U(1)$ basis. Due to the incompatibility of the two sublattice structures in (b), one needs to introduce four HP bosons corresponding to the four sublattice structures A, B, C, D to perform the spin wave expansion to any order. Due to the four sublattice structures, the RBZ is four times smaller than the full BZ.

or Dresselhaus SOC, we identify a new spin–orbital entangled commensurate ground state called the Y-y state[5] subject to quantum fluctuations at $T = 0$. We evaluate the quantum fluctuations by spin wave expansions up to $1/S^2$ order (which is also called the $1/S$ correction to the linear spin wave expansion (LSWE) in the previous literature on Heisenberg models). It supports a massive relativistic commensurate magnon C-C_0 in one SOC parameter regime and an incommensurate magnon C-IC in the other regime (see footnote 6). The two gap minima positions of the C-IC magnons are continuously tuned by the SOC strength. At low temperatures, these magnons dominate all the physical quantities such as the specific heat, magnetization, $(0, \pi)$ and $(\pi, 0)$ susceptibilities, Wilson ratio and also various spin correlation functions. At $T = 0$, the longitudinal spin structure factor shows a sharp peak at $\mathbf{k} = 0$ in the reduced Brillouin zone (RBZ) reflecting the ground state. However, the transverse spin structure factor displays non-trivial features reflecting the magnon excitations above the ground state. The C-C_0 leads to a pinned central Lorentzian peak at $\mathbf{k} = 0$ in the transverse spin structure factor. However, the C-IC splits it into two Lorentzian peaks located at its two gap minima, while changing its structure at $\mathbf{k} = 0$ into a saddle point one. In the weak coupling limit, any weak repulsive interaction leads to a weak Y-y state which also hosts low energy fermionic excitations. There is a crossover from weak to strong coupling where the fermionic excitation energies increase. The electronic and spin Wilson loops can be determined by measuring specific heats in the high temperature expansion in the weak and strong coupling limit, respectively. The C-IC encodes short-range incommensurate seeds embedded in an commensurate ground state at $T = 0$, which justifies its name (see footnote 6). The crucial roles to be played by these seeds at generic SOC parameters (α, β) and under various external probes are outlined in the conclusion section. Experimental realizations and detections in both layered noncentrosymmetric materials and cold atom systems are discussed.

2. The interacting fermionic model, the quantum spin model in the strong coupling limit and exact symmetry analysis

The tight-binding Hamiltonian of spin 1/2 fermions at half filling hopping in a 2D square optical lattice subject to any combination of Rashba and Dresselhaus SOC is:

$$\mathcal{H}_f = -t\sum_{\langle ij\rangle}(c^\dagger_{i\sigma}U^{\sigma\sigma'}_{ij}c_{j\sigma'} + \text{h.c.}) + U\sum_i\left(n_{i\uparrow} - \frac{1}{2}\right)\left(n_{i\downarrow} - \frac{1}{2}\right) \tag{1}$$

where t is the hopping amplitude along the nearest neighbors $\langle ij\rangle$, the non-Abelian gauge fields $U_{ii+\hat{x}} = \mathrm{e}^{\mathrm{i}\alpha\sigma_x}$, $U_{ii+\hat{y}} = \mathrm{e}^{\mathrm{i}\beta\sigma_y}$ are put on the two links in figure 1(a) which is the lattice regularization of the linear combination

[5] Here we still use the same notation used in [25]. In the Y-$(0, \pi)$ called Y-y state, the first letter indicates the spin polarization, the second letter indicates the orbital order. In the C-C_0 magnons, the first letter indicates that the ground state is commensurate, the second letter indicates that the excitation is also commensurate with its minimum at $\boldsymbol{k} = 0$. In the C-IC magnons, the first letter indicates the ground state is still commensurate, the second letter indicates the excitation is incommensurate with its minimum at incommensurate momenta $\boldsymbol{k} = (0, \pm k_y^0)$. By the SOC in equation (2) which, in fact, is a spin only model, we mean the spin–bond coupling in the same sense as in the Kitaev honeycomb lattice model, namley, the spin–spin exchange interaction is bond-dependent in the form of the two $SO(3)$ rotation matrices $R(\hat{x}, 2\alpha)$, $R(\hat{y}, 2\beta)$ in equation (2). For example, the celebrated Kitaev model has three bond-dependant spin–spin interactions.

$k_x\sigma_x + k_y\sigma_y$ of the Rashba and Dresselhaus SOC in a continuum momentum space [8, 11]. $\alpha = \pm\beta$ stands for the isotropic Rashba (Dresselhaus) case. $U > 0$ is the Hubbard onsite interaction.

In the strong coupling limit $U/t \gg 1$, to the order $O(t^2/U)$, we obtain the effective spin 1/2 RAFHM:

$$\mathcal{H}_{RH} = J\sum_i [S_i^a R_{ab}(\hat{x}, 2\alpha) S_{i+\hat{x}}^b + S_i^a R_{ab}(\hat{y}, 2\beta) S_{i+\hat{y}}^b] \tag{2}$$

with the antiferromagnetic exchange interaction $J = 4t^2/U > 0$, $a, b = 1, 2, 3$ are the three components of the spin operator, the $R(\hat{x}, 2\alpha)$, $R(\hat{y}, 2\beta)$ are the two SO(3) rotation matrices around the X and Y spin axis by angle 2α, 2β putting on the two bonds along $\hat{x}$, $\hat{y}$, respectively.

Here, we plan to study the quantum or topological phenomena in the RAFHM at generic (α, β). However, it is a very difficult task, so we take a 'divide and conquer' strategy. First, we identify a solvable line $(\alpha = \pi/2, \beta)$ and explore new and rich quantum phenomena along the line. Then starting from the results achieved from the solvable line, we will investigate the quantum phenomena at the generic (α, β) including the Rashba or Dresselhaus SOC point $\alpha = \pm\beta$. In this paper, we will focus on the first task. The second task will be outlined in the conclusion section and presented in detail elsewhere. In the past, this type of 'divide and conquer' approach has been very successful in solving many quantum spin models. For example, in the single (multi-) channel Kondo model, one solves the Thouless (Emery–Kivelson) line [21, 22], then do perturbations away from it. In the quantum-dimer model, one solves the Rohksa–Kivelson (RK) point which shows spin liquid physics [23], then one can study the effects of various perturbations away from it [24]. Recently, this 'divide and conquer' strategy was quite successfully applied to study the rotated ferromagnetic Heisenberg model (RFHM) along the solvable line first in [25], then at the generic SOC parameter in [26].

The general approach to investigate an interesting model is to first present an exact symmetry analysis which will lead to some non-trivial exact results which will put constraints on any specific calculations such as the systematic spin wave calculations in terms of $1/S$ to be performed in this paper. At a generic (α, β), the fermionic model equation (1) has time reversal symmetry $\mathcal{T}$: $\mathbf{k} \to -\mathbf{k}$, $\mathbf{S} \to -\mathbf{S}$, translational symmetry and three spin–orbital coupled Z_2 symmetries: (1) $\mathcal{P}_x$ symmetry: $S^x \to S^x$, $k_y \to -k_y$, $S^y \to -S^y$, $S^z \to -S^z$. (2) $\mathcal{P}_y$ symmetry: $S^y \to S^y$, $k_x \to -k_x$, $S^x \to -S^x$, $S^z \to -S^z$. (3) $\mathcal{P}_z$ symmetry: $k_x \to -k_x$, $S^x \to -S^x$, $k_y \to -k_y$, $S^y \to -S^y$, $S^z \to S^z$ which is also equivalent to a joint π rotation of both the spin and the orbital around the $\hat{z}$ axis. At the Rashba or Dresselhaus point $\alpha = \pm\beta$, the $\mathcal{P}_z$ symmetry is enlarged to the spin–orbital coupled symmetry $C_4 \times C_4$ which is a joint $\pi/2$ rotation of both the spin and the orbital around the $\hat{z}$ axis. Along the line $(\alpha = \pi/2, \beta)$, there is also an enlarged spin–orbital coupled $U(1)_{\rm soc}$ symmetry $[H_{\rm f}, \sum_{\rm i}(-1)^{\rm i_x} c_{\rm i}^\dagger \sigma^y \sigma_{\rm i}] = 0$. Of course, at the two Abelian points, the $U(1)_{\rm soc}$ symmetry is enlarged to the $SU(2)$ symmetry in the corresponding rotated basis.

The RAFHM equation (2) inherits all the symmetries of the fermionic model equation (1). Along the line $(\alpha = \pi/2, \beta)$, in addition to the spin–orbital coupled $U(1)_{\rm soc}$ symmetry $[H_{\rm f}, \sum_{\rm i}(-1)^{\rm i_x} c_{\rm i}^\dagger \sigma^y \sigma_{\rm i}] = 0$, it also has an extra mirror $\mathcal{M}$ symmetry: under the local rotation $\tilde{\mathbf{S}}_i = R(\hat{x}, \pi)R(\hat{y}, \pi n_2)\mathbf{S}_i$, then followed by a time reversal transformation, $\beta \to \pi/2 - \beta$. At the middle point $\beta = \pi/4$, the Hamiltonian is invariant under such a mirror transformation.

The gauge invariant fermionic Wilson loop around an elementary square is the same as the bosonic case [25] $W_f = 2 - 4\sin^2\alpha \sin^2\beta$ which stands for the non-Abelian flux through the square. The R-matrix Wilson loop W_R around a fundamental square is defined as $W_R = \mathrm{Tr}[R_x R_y R_x^{-1} R_y^{-1}] = (W_f)^2 - 1$ which can be used to characterize the equivalent class and frustrations in the RAFHM equation (2) The $W_R = 3$ $(W_R < 3)$ stands for the Abelian (non-Abelian) points. The relations between two sets of Wilson loops are in two-to-one relation due to the coset $SU(2)/Z_2 = SO(3)$.

At the two ends of the line $\beta = 0$ and $\beta = \pi/2$, we get the antiferromagnetic Heisenberg model in the rotated basis $H = J\sum_{\rm ij} \tilde{\mathbf{S}}_{\rm i} \cdot \tilde{\mathbf{S}}_{\rm j}$ where $\tilde{\mathbf{S}}_{\rm i} = R(\hat{x}, \pi {\rm i_x})\mathbf{S}_{\rm i}$ and $H = J\sum_{\rm ij} \tilde{\tilde{\mathbf{S}}}_{\rm i} \cdot \tilde{\tilde{\mathbf{S}}}_{\rm j}$ where $\tilde{\tilde{\mathbf{S}}}_{\rm i} = R(\hat{x}, \pi {\rm i_x})R(\hat{y}, \pi {\rm i_y})\mathbf{S}_{\rm i}$, respectively. So the Hamiltonian has SU(2) symmetry in the rotated basis $S\tilde{U}(2)$ or $S\tilde{\tilde{U}}(2)$, respectively. Transferring back to the original basis, the SU(2) symmetry is generated by $\sum_i S_i^x$, $\sum_i(-1)^{i_x} S_i^y$, $\sum_i(-1)^{i_x} S_i^z$ at $\beta = 0$ and by $\sum_i(-1)^{i_y} S_i^x$, $\sum_i(-1)^{i_x} S_i^y$, $\sum_i(-1)^{i_x+i_y} S_i^z$ at $\beta = \pi/2$, respectively. Both contain the conserved quantity $\sum_i(-1)^{i_x} S_i^y$. In fact, as mentioned above [25], the spin–orbital coupled $U(1)_{\rm soc}$ symmetry $[H_{\rm RH}, \sum_{\rm i}(-1)^{\rm i_x} S_{\rm i}^y] = 0$ extends along the whole line $(\alpha = \pi/2, \beta)$ connecting the two Abelian points. In section 5, we will also perform spin wave calculations in the rotated basis $S\tilde{U}(2)$.

As expected, the RAFHM with $J > 0$ should display dramatically different physics to the RFHM model with $J < 0$ studied in [25]. In the classical limit $S \to \infty$, one can show that the ground state is the Y-y state in

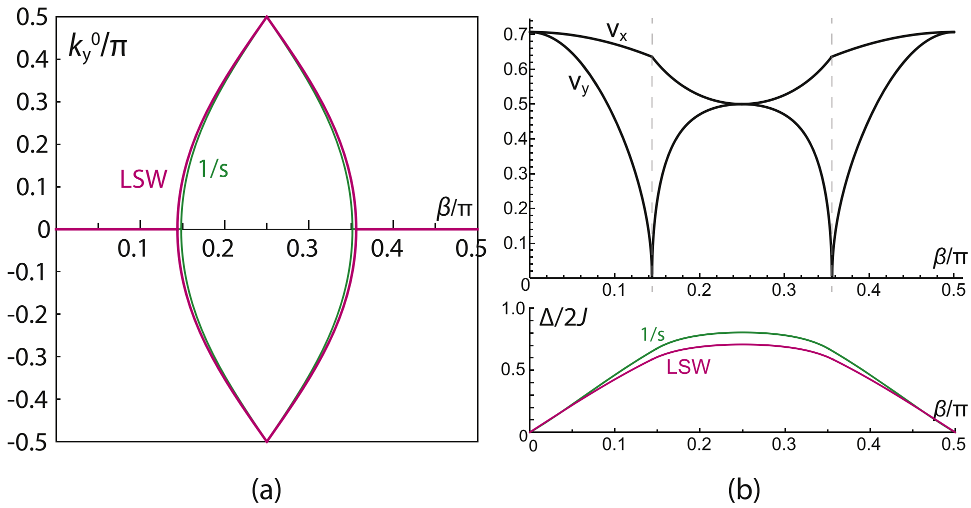

Figure 2. (a) The minima position $\mathbf{k} = (0, \pm k_y^0)$ of the relativistic magnons in the RBZ. (b) The energy gap (or mass) $\Delta(\beta)$ at the minima in (a) with the two magnon velocities $v_x \geqslant v_y$. The equality holds at $\beta = 0, \pi/4, \pi/2$. Near β_i, $i = 1, 2$, v_x has a cusp, while $v_y \sim |\beta - \beta_i|^{1/2}$. The LSWE ($1/S$ order) results are the purple line and $1/S$ corrections to LSWE the green line. The $1/S$ corrections are found to be small (see appendix B).

figure 1(a) which still respects both the $U(1)_{\mathrm{soc}}$ symmetry and the $\mathcal{M}$ symmetry[6]. Note that the $\mathcal{M}$ symmetry will be used to classify the symmetry of the minimum positions and the magnon gap in figure 2. The Y-y state also keeps the $\mathcal{P}_y$ and $\mathcal{TP}_x$ and $\mathcal{TP}_z$ symmetries.

3. The C-C_0 and C-IC magnons above the Y-y state

Based on the Y-y state in figure 1(a), we introduce the Holstein–Primakoff (HP) bosons a and b for the sublattices A and B, respectively. The Hamiltonian equation (2) can be written in a systematic $1/S$ expansion in terms of the HP bosons [27–30]:

$$\mathcal{H}_{\mathrm{spin}} = \mathcal{H}_0 + 2JS(\mathcal{H}_2 + \mathcal{H}_4 + \cdots) \tag{3}$$

where $\mathcal{H}_0 = -2NJS^2$ is the classical ground state energy. $\mathcal{H}_2$ represents linear spin wave theory, $\mathcal{H}_4$ represents the $1/S$ correction to linear spin wave theory [29] and so on. In the rest of the paper, we will use $2JS$ to be the energy unit.

By combining a unitary transformation, followed by a Bogoliubov transformation (see appendix A), one can diagonalize $\mathcal{H}_2$:

$$\mathcal{H}_2 = \sum_k (\omega_k^+ + \omega_k^- - 2) + 2\sum_k (\omega_k^- \alpha_k^\dagger \alpha_k + \omega_k^+ \beta_k^\dagger \beta_k) \tag{4}$$

where the LSWE spectrum $\omega_k^\pm = \sqrt{1 - (\gamma_k^\pm)^2}$ and $2\gamma_k^\pm = \cos 2\beta \cos k_y \pm \sqrt{\cos^2 k_x + \sin^2 2\beta \sin^2 k_y}$. When $\beta < \pi/4$, $\omega_k^+ < \omega_k^-$, when $\beta > \pi/4$, $\omega_k^+ > \omega_k^-$, at $\beta = \pi/4$, $\omega_k^+ = \omega_k^-$. So ω_k^+ and ω_k^- are related by $\mathcal{M}$ symmetry. In the following, for notational simplicity, we call the lower branch ω_k^-, the energy is measured in the unit of $4JS$.

Along the line ($\alpha = \pi/2$, $0 < \beta < \pi/2$), the position of the minima of the lower branch ω_k^- is given in equation (A.5) and shown in figure 2(a). One can see that when $0 < \beta < \beta_1$ and $\beta_2 = \pi/2 - \beta_1 < \beta < \pi/2$, the Y-y ground state supports the C-C_0, when $\beta_1 < \beta < \beta_2$, it supports the C-IC magnons. The low energy excitation can be obtained from the expansion around the minima $\mathbf{k} = \mathbf{k}_0 + \mathbf{q}$ as:

$$\omega_q^- = \sqrt{\Delta^2(\beta) + v_x^2 q_x^2 + v_y^2 q_y^2} \tag{5}$$

where the mass Δ at the minima and the two velocities are given in equation (A.7) and shown in figure 2(b).

[6] In appendix A of [25], we showed that the exact ground state along ($\alpha = \pi/2$, β) in the RFHM is the Y-x state (see footnote 6). Applying $(-1)^{x+y}$ to the Y-x state leads to the Y-y state which is only the classical ground state of the RAFHM along the same line. More straightforwardly, from the RAFHM model equation (2) along the line, one can see only the Y-y state can minimize the bond energies along both $\hat{x}$ and $\hat{y}$ bonds. This is also the reason why this line is special, because it is the only line which supports a collinear state in the 2D SOC parameter space [26]. See also the caption of figure 8 for another intuitive explanation why the Y-y state is the classical ground state along the line.

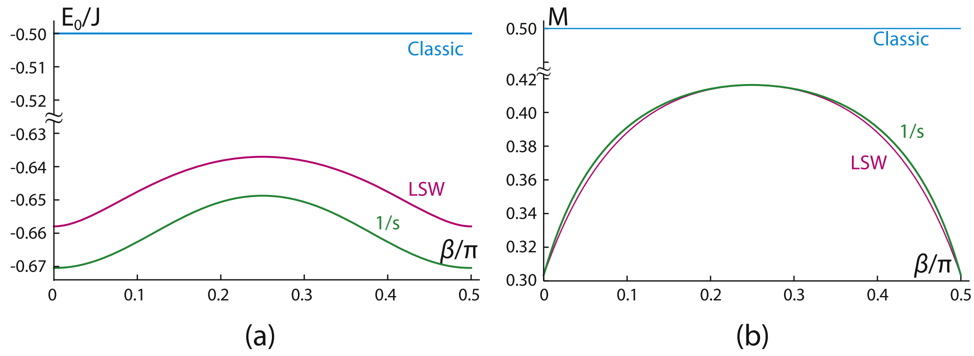

Figure 3. (a) The ground-state energy and (b) the magnetization as a function of gauge field parameter $0 < \beta < \pi/2$ along the line. Shown are the classical results in blue color (flat line on top) which are independent of β, LSWE ($1/S$ order) by the purple line and $1/S$ corrections to LSWE by the green line. There are always $1/S$ corrections to the ground state energy in (a). In (b), it vanishes at the two Abelian points $\beta = 0, \pi$ and also at $\beta = \pi/4$. The $1/S$ corrections are found to be small in both quantities. This fact shows that the LSWE is quite accurate even for the smallest $s = 1/2$ which hosts the largest quantum fluctuations.

Thus, they are relativistic gapped particles with a gap Δ and two velocities $v_x \geqslant v_y$ where the equality holds at $\beta = 0, \pi/4, \pi/2$ near β_i, $i = 1, 2$, $v_y \sim |\beta - \beta_i|^{1/2}$. In sharp contrast, the C-IC magnons in the RFHM [25] are non-relativistic gapped particles with a gap Δ and two effective masses $m_y \geqslant m_x$.

At the two Abelian points $\beta = 0, \pi/2$, the system has SU(2) symmetry in the rotated basis $S\tilde{U}(2)$ with $\mathbf{S}_i = R(\hat{x}, \pi i_x)R(\hat{y}, \pi i_y)\mathbf{S}_i$ and $S\tilde{\tilde{U}}(2)$ and $S\tilde{\tilde{U}}(2)$ with $\mathbf{S}_i = R(\hat{x}, \pi i_x)R(\hat{y}, \pi i_y)\mathbf{S}_i$ respectively (figure 8), and equation (4) reduces to the antiferromagnetic spin wave $\omega_k \sim k$ at the minima $(0, 0)$ and $(\pi, 0)$, respectively.

We also obtain the ground-state energy and the magnetization at $T = 0$ from the LSWE:

$$E_{\mathrm{GS}} = 2NJS^2 + 2JS\sum_k(\omega_k^+ + \omega_k^- - 2)$$
$$M = S - \frac{1}{2N}\sum_k\left(\frac{1}{\omega_k^+} + \frac{1}{\omega_k^-} - 2\right) \quad (6)$$

which are drawn in figure 3.

4. Thermodynamic quantities at low temperatures

At low temperatures, one can drop the higher energy mode of the ω_k^+ and evaluate the specific heat and the staggered magnetization of the Y-y state in figure 4 due to the relativistic magnons:

$$C_m(T) \sim \frac{\Delta^3}{2\pi v_x v_y T}e^{-\Delta/T} \quad M(T) \sim M - \frac{T^2}{2\pi v_x v_y}e^{-\Delta/T} \quad (7)$$

where M is the zero temperature staggered magnetization listed in equation (6).

By coupling to the conserved quantity $-H_s\sum_i(-1)^{i_x}S_i^y$ and to the order parameter $-H_s\sum_i(-1)^{i_y}S_i^y$, respectively, one can also evaluate the $(\pi, 0)$ and $(0, \pi)$ staggered susceptibilities:

$$\chi_{(\pi,0)}(T) \sim \frac{\Delta}{2\pi v_x v_y}\mathrm{e}^{-\Delta/T} \quad \chi_{(0,\pi)}(T) \sim \chi_{(0,\pi)}(T=0) - \frac{1}{2\pi v_x v_y}\frac{1}{\Delta}\mathrm{e}^{-\Delta/T} \quad (8)$$

where $\chi_{(0,\pi)}(T=0) = \sum_{k,s=\pm}\frac{1-(\omega_k^s)^2}{2(\omega_k^s)^3}$ is the zero temperature $(0, \pi)$ staggered susceptibility.

From the specific heat $C_m(T)$ in equation (7) and the conserved $(\pi, 0)$ staggered susceptibility $\chi_{(\pi,0)}(T)$ in equation (8), one can form the Wilson ratio:

$$R_w = \frac{T\chi_{(\pi,0)}(T)}{C_m(T)} = \left(\frac{T}{\Delta}\right)^2 \quad (9)$$

which only depends on[7] the dimensionless quantity of $T/\Delta(\beta)$.

The physical quantities in equations (7) and (8) depend explicitly on the magnon's two velocities v_x, v_y and its gap Δ shown in figure 2(b). However, the Wilson ratio in equation (9) only depends on the gap Δ. It is easy to see that the longitudinal spin structure factor always has a very sharp peak $M^2\delta_{\mathbf{k},0}$ at the ordering wavevector

[7] At β_1, β_2, from $v_y \sim |\beta - \beta_i|^{1/2}$ and a simple scaling analysis, one can just set $v_y \sim T^{1/4}$ in all the physical quantities in equations (7) and (8). The Wilson ratio stays the same.

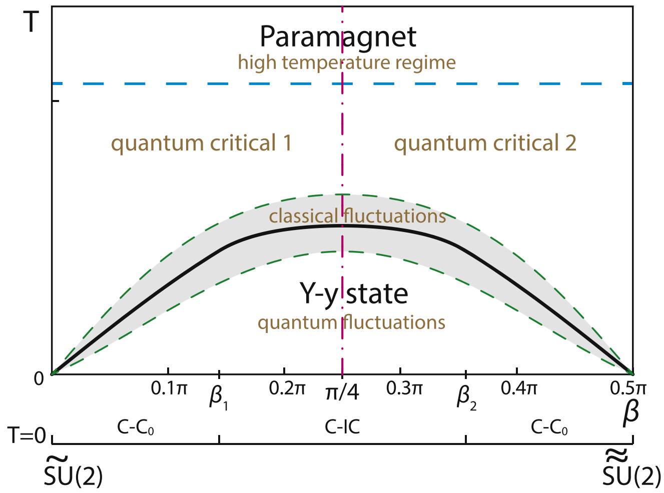

Figure 4. The classical fluctuations dominate in the narrow regime around the finite temperature transition denoted by the two dashed lines, so it is still in the 2D Ising transition class as that in the RFHM. The quantum fluctuations dominate in the Y-y state below the dashed line, which is the focus of section 4. The QC1 and QC2 regime where $\Delta \ll T$ are controlled by the two Abelian points at $\beta = 0$ and $\beta = \pi/2$ respectively, are dominated by the quantum antiferromagnetic fluctuations in the $\tilde{\mathbf{SU}}(2)$ and $\tilde{\tilde{\mathbf{SU}}}(2)$ basis, respectively. The high temperature expansion in section 7 holds only in the high temperature regime above the blue dashed line.

$(0, \pi)$ (which is at $(0, 0)$ in the RBZ) of the Y-y state in figure 1(a) with the spectral weight equal to the square of the magnetization. Unfortunately, the positions of the gap minima at $(0, k_y^0)$ of the C-IC magnons in figure 2(a) cannot be reflected in all these physical quantities. In the following, we show that they can be precisely mapped out by the peak positions in the transverse structure factors.

5. Transverse structure factors in the rotated basis $S\tilde{U}(2)$ (also called $U(1)$ basis)

Performing a local gauge transformation $\tilde{c}_i = (i\sigma_x)^{i_x} c_i$ on equation (1), one can get rid of the gauge fields on all the x-links and all the remaining gauge fields on the y-links commute. Similarly, by performing a local rotation $\tilde{\mathbf{S}}_n = R(\hat{x}, \pi n_1)\mathbf{S}_n$ in equation (2), one can get rid of the R-matrix on the x-links shown in figure 1(b1). It makes the $U(1)_{\rm soc}$ symmetry with the conserved quantity $Q_c = \sum \tilde{S}_i^y$ explicit in the rotated basis $S\tilde{U}(2)$ (also called $U(1)$ basis), but at the expense of reaching the translational symmetry broken Hamiltonian with the $(\pi, 0)$ sublattice structure in figure 1(b1). The Y-y ground state in the original basis in figure 1(a) becomes the Y-(π, π) Néel state in the $U(1)$ basis in figure 1(b2). Because of the incompatibility of the two sublattice structures in figure 1(b), one needs to introduce four HP bosons a, b, c, d corresponding to the four sublattice structures A, B, C, D shown in figure 1(b2) respectively to perform the spin wave expansion to any order.

Several physical quantities such as the magnitude of the magnetization $M_Q(T)$, specific heat C_m, the gaps Δ and density of state (DOS) are gauge invariant, so are the same in both bases. The $(\pi, 0)$ and $(0, \pi)$ susceptibilities become the uniform and the (π, π) staggered susceptibilities respectively in the $U(1)$ basis. The Wilson ratio is also gauge invariant after using the uniform susceptibility in the $U(1)$ basis. However, the spin–spin correlation functions are gauge dependent [31][8]. As shown in this section, it is the spin–spin correlations in the $U(1)$ basis which can map out the C-C_0 and C-IC relativistic magnons most efficiently [25]. Due to the explicit $U(1)$ symmetries in the $U(1)$ basis, the anomalous structure factors $S^{++} = S^{--} = 0$, so one needs only evaluate the normal structure factors S^{+-}. However, due to the four sublattice structure in figure 1(b2), one needs to evaluate it at four different orbital orders at $\mathbf{Q}_u = (0, 0)$, $\mathbf{Q}_x = (\pi, 0)$, $\mathbf{Q}_y = (0, \pi)$, $\mathbf{Q}_s = (\pi, \pi)$. Due to the exact relations among them in the RBZ:

$$S_u^{+-}(\mathbf{k}) = S_s^{+-}(\mathbf{k} + \mathbf{Q}_s) = S_{\mathbf{Q}_x}^{+-}(\mathbf{k} + \mathbf{Q}_x) = S_{\mathbf{Q}_y}^{+-}(\mathbf{k} + \mathbf{Q}_y) \tag{10}$$

one can combine them into a single structure factor in the EBZ: $0 < k_x, k_y < 2\pi$

$$S_{EBZ}^{+-}(k) = \sum_{s=\pm} \frac{[1 + (-1)^s \sin\theta_k](1 - \gamma_k^s)}{\omega_k^s} \tag{11}$$

[8] As stressed in this work, in contrast to condensed matter systems where only gauge invariant quantities can be measured, both gauge invariant and non-invariant quantities can be measured in cold atom systems by experimentally generating various non-Abelian gauges corresponding to the same set of Wilson loops. See also [25].

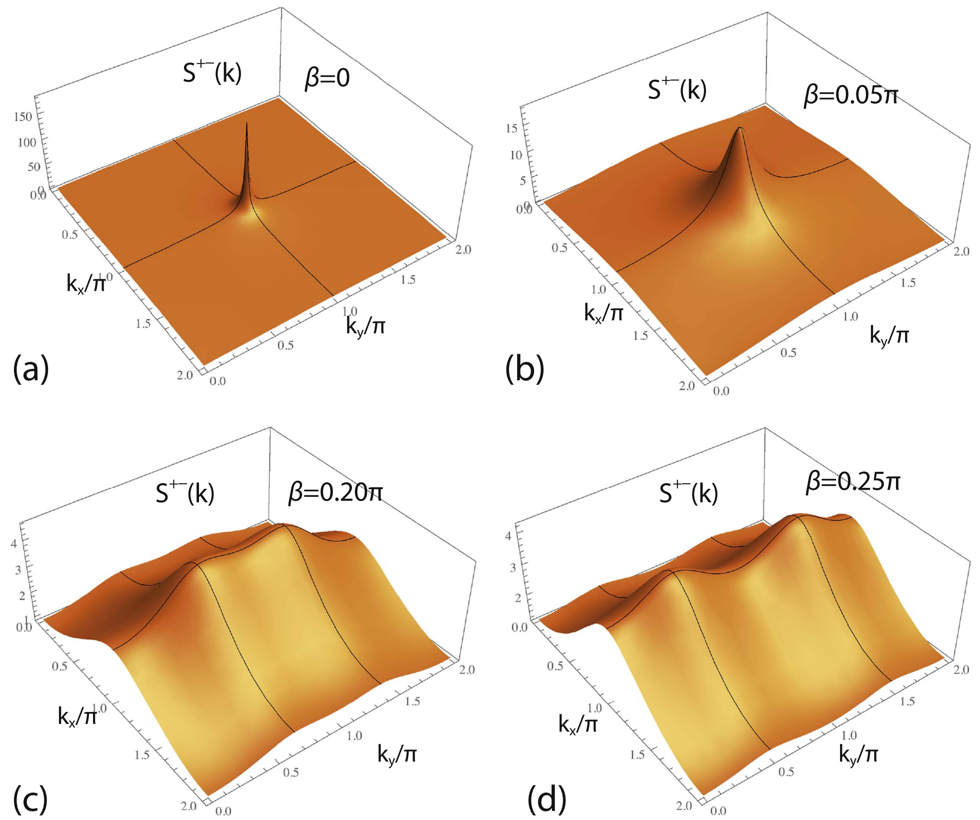

Figure 5. Transverse structure factor $S^{+-}(\mathbf{k})$ at $T = 0$ in the $U(1)$ basis at the extended BZ. When $\beta = 0$ (Abelian point), 0.05π (C-C_0 magnons), there is a central peak at (π, π) in a Lorentzian form. When $\beta = 0.20\pi$, $\pi/4$ (C-IC magnons), the central Lorentzian peak splits into two Lorentzian ones peaked around $(\pi, \pi \pm k_y^0)$ whose fine structures are shown in figure 6. The longitudinal structure factor always shows a sharp peak at the ordering wavevector (π, π) in figure 1(b2).

where the denominator is precisely the relativistic magnons spectrum ω_k^s listed below equation (4), the numerator contains γ_k^s listed below equation (4) and $\sin\theta_k$ is given in the unitary transformation equation (A.2) in appendix A.

The transverse structure factor equation (11) at several typical β is shown in figure 5 and its fine structure near $\beta = \pi/4$ is shown in figure 6. When $0 < \beta < \beta_1$ or $\beta_2 < \beta < \pi/2$, C-C_0 leads to a central peak at $\mathbf{k} = (\pi, \pi)$. At the Abelian point $\beta = 0$ in figure 5(a), $S^{+-}(q) \sim \frac{\sqrt{2}}{q}$ where $k = (\pi, \pi) + q$. Obviously, the singularity at (π, π) is due to the infrared divergence of the Goldstone mode $\omega = ck$ in equation (11). At a small β in the C-C_0 regime in figure 5(b):

$$S^{+-}_{\text{C-C}_0}(q) \sim \frac{1}{\sqrt{v_x^2 q_x^2 + v_y^2 q_y^2 + \Delta^2(\beta)}} \tag{12}$$

where the $\Delta(\beta) \sim \sqrt{2}\beta$ is the gap opening due to the small β listed in equation (A.7) and shown in figure 2(b).

In figure 5(c), when $\beta_1 < \beta < \beta_2$, the C-IC starts to split the central peak into two peaks located around its two minima $\mathbf{k} = (\pi, \pi \pm k_y^0)$ shown in figure 2(a), the $\mathbf{k} = (\pi, \pi)$ becomes a saddle point being maximum along the k_x direction, minimum along the k_y direction. In figure 5(d), at $\beta = \pi/4$, the two peaks are exactly located at the two minima $(\pi, \pi \pm \frac{\pi}{2})$ of the C-IC shown in figure 2(a). Each of the two well separated Lorentzian peaks is given by:

$$S^{+-}_{\text{C-IC}}(q) \sim \frac{3/2}{\sqrt{(q_x^2 + q_y^2)/4 + 1/2}} \tag{13}$$

where $\Delta(\beta = \pi/4) = 1/2$ is the largest gap at $\beta = \pi/4$ shown in figure 2(b). As shown in figure 6, the two Lorentzian peaks are moving closer when $\beta < \pi/4$ or apart when $\beta > \pi/4$. So in the C-IC regime, the structure factor maps out precisely the dispersions of the C-IC relativistic magnons which are completely due to quantum fluctuations and intrinsically embedded in the quantum Y-y ground state at $T = 0$.

It is constructive to contrast with RFHM where the sublattice structure of the transformed Hamiltonian $(\pi, 0)$ is compatible with the classical ferromagnetic state in the $U(1)$ basis [25], so one need only introduce two HP bosons to perform spin wave expansion. So one only needs to form a uniform $S_u^{+-}(k)$ and a $(\pi, 0)$ staggered

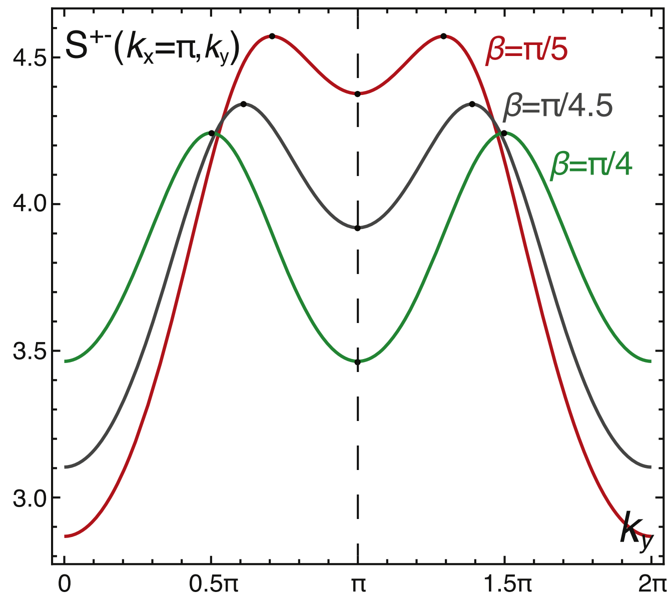

Figure 6. Cross section ($k_x = \pi$, k_y) of the transverse structure factor $S^{+-}(\mathbf{k})$ of the C-IC near $\beta = \pi/4$ in figure 5. At $\beta = \pi/4$, there are two well separated Lorentzian peaks exactly at $(\pi, \pi \pm \pi/2)$. When $\beta < \pi/4$, the two Lorentzian peaks move closer to each other. When $\beta > \pi/4$, they move apart as dictated by the mirror symmetry (not shown for clarity).

transverse structure factor $S_s^{+-}(k)$ in the RBZ listed in equation 31 in [25]. One can also establish the exact relation $S_u^{+-}(k) = S_s^{+-}(k + (\pi, 0))$, so one can combine them into a single structure factor in the EBZ. It is a Gaussian exponentially suppressed by $e^{-\Delta/T}$, peaked at $(0, \pm k_y^0)$ with a temperature dependent width $\sigma_x = \sqrt{m_x(\beta)T}$ due to the thermal fluctuations at a finite T. This is because there is no quantum fluctuations at $T = 0$. The Y-x state is an exact eigenstate. The C-IC magnons do NOT exist at $T = 0$, so they need to be thermally excited, so can only be detected at a finite T.

6. Weak coupling Y-y state, low energy fermionic excitations and weak to strong crossover

So far, we have focused on the strong coupling expansion at $U \gg t$ where the RAFHM equation (2) holds and the charge degree of freedoms are frozen. It is also important to start from the weak coupling limit $U \ll t$ where one needs to also consider charge fluctuations and study how it approaches the strong coupling limit. Using the identity $n_{i\uparrow}n_{i\downarrow} = \frac{1}{2}n_i - \frac{2}{3}\mathbf{S}_i^2$ to explicitly keep the spin SU(2) symmetry of the Hubbard interaction in equation (1), one can introduce a magnetic order parameter $\mathbf{M}_i$ to decouple the interaction term:

$$\mathcal{H}_{\mathbf{M}} = -t\sum_{\langle i,j\rangle}(c_{i\sigma}^\dagger U_{ij}^{\sigma\sigma'}c_{j\sigma'} + \text{h.c.}) + \frac{3}{8U}\sum_i \mathbf{M}_i^2 + \sum_i \mathbf{M}_i\cdot\mathbf{S}_i. \tag{14}$$

The evolution of the non-interacting Fermi surfaces (FS) along the line $(\alpha = \pi/2, \beta)$ is shown in figure 7(a). Due to the FS nesting conditions at the half-filling shown in figure 7, any weak interaction will open gaps to the non-interacting FS when $\beta \neq \pi/2$. So one can perform a well controlled weak coupling analysis to determine the spin–orbit orders of the ground state and also the excitation spectra.

From the FS geometry in figure 7(a), there can only be four possible orbital orders $\mathbf{Q}_1 = (0, 0)$, $\mathbf{Q}_2 = (\pi, 0)$, $\mathbf{Q}_3 = (0, \pi)$, $\mathbf{Q}_4 = (\pi, \pi)$. Substituting the order parameter $\mathbf{M}_i = \mathbf{M}e^{i\mathbf{Q}\cdot\mathbf{r}_i}$ where $\mathbf{Q} = \mathbf{Q}_i$, $i = 1, 2, 3, 4$ and $\mathbf{M} = (X, Y, Z)$ into equation (14) leads to the mean field Hamiltonian: $H_{MF} = H_0 + \frac{3N|\mathbf{M}|^2}{8U}$ and

$$H_0 = \frac{1}{2}\sum_k \begin{pmatrix} c_k^\dagger & c_{k+Q}^\dagger \end{pmatrix} \begin{pmatrix} T_k & M^a\sigma^a \\ M^a\sigma^a & T_{k+Q} \end{pmatrix} \begin{pmatrix} c_k \\ c_{k+Q} \end{pmatrix} \tag{15}$$

where $T_k = -4t[\cos\beta\cos k_y - \sigma^x \sin k_x - \sigma^y \sin\beta \sin k_y]$ is the kinetic part of H_0 encoding the SOC parameters $(\alpha = \pi/2, \beta)$.

For $\mathbf{Q}_3 = (0, \pi)$, diagonalizing the 4×4 matrix in equation (15) leads to four fermionic energy levels $\pm\epsilon_1, \pm\epsilon_2$. It is an insulating state with P-H symmetry. Due to the lack of spin $SU(2)$ symmetry, the minimization procedures are much more involved than those with the symmetry. We also take the 'divide and conquer'

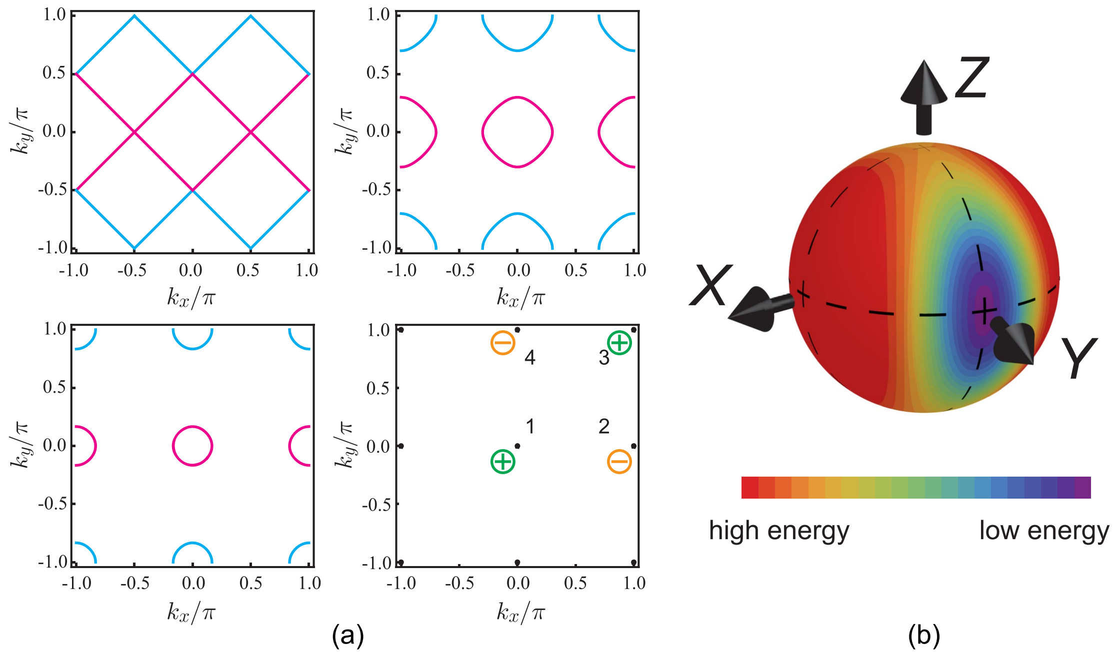

Figure 7. (a) The FS evolves along the line ($\alpha = \pi/2$, β) at $\beta = 0, \pi/5, 2\pi/5, \pi/2$. At $\beta = \pi/2$, there are four Dirac fermions located at $\mathbf{K}_1 = (0, 0)$, $\mathbf{K}_2 = (\pi, 0)$, $\mathbf{K}_3 = (\pi, \pi)$ and $\mathbf{K}_4 = (\pi, 0)$ labeled as $1, 2, 3, 4$ with the topological winding numbers ± 1. There are FS nesting away from $\beta = \pi/2$. Purple (green) is particle (hole) surface. (b) The ground-state energy as a function of magnetic orientation $\mathbf{M} = (X, Y, Z)$ at the orbital order $\mathbf{Q} = (0, \pi)$ with the parameter $U = 0.2t$, $\beta = \pi/6$. The position on the sphere indicates the spin orientation. Red (purple) color means higher (lower) energy. The figure shows that the Y spin-orientation is the ground state at the orbital order $\mathbf{Q} = (0, \pi)$. In fact, the Y-y state is the global ground state when considering all the other possible orbital orderings.

strategy: first fixing the spin orientation and finding the optimal magnitude and energy in the subspace, then determining the optimal orientation and magnitude. The results for the general spin orientation $\mathbf{M} = (X, Y, Z)$ are shown in figure 7(b). The global ground state has $(0, Y, 0)$ spin orientation; it is nothing but the Y-y state which respects the $U(1)_{\mathrm{soc}}$ symmetry. It also supports two branches of gapped fermionic excitations listed in equation (D.1). By repeating the calculations for $\mathbf{Q}_4 = (\pi, \pi)$, we find the lowest spin-orientation is X-(π, π) which breaks the $U(1)_{\mathrm{soc}}$ symmetry. By applying the $U(1)_{\mathrm{soc}}$ symmetry operator, one can see X-(π, π) is degenerate with Z-$(0, \pi)$ which, of course, has higher energy than the $U(1)_{\mathrm{soc}}$ symmetric Y-y state as shown in figure 7(b).

For $\mathbf{Q}_2 = (\pi, 0)$ or $(0, 0)$, it is the magnetic ordering in the P-P channel or hole-hole (H-H) channel, so breaks P-H symmetry. Both need a finite $U_c > 0$ to reach a metallic state with only partial fillings of all four fermionic bands ϵ_i, $i = 1, 2, 3, 4$. It has much higher energies than those insulating states in the P-H channel. So we conclude that the Y-y state is indeed the global ground state at weak coupling.

As shown in figure 8, due to the $S\tilde{U}(2)$ and $S\tilde{\tilde{U}}(2)$ symmetry at the two Abelian points $\beta = 0, \pi/2$ respectively, the Y-y state is degenerate with the other two states. However, away from them, the FS nesting conditions in figure 7 at half-filling favors the Y-y state which also supports the low energy fermionic excitations in equation (D.1). So the specific heat in equation (7) will also receive the contributions from the fermionic part.

Following the procedures in [50], splitting the magnetic fluctuations into one longitudinal and two transverse components and performing Gaussian fluctuations above the Y-y state, we can also identify the C-C_0 and C-IC magnons from the poles of the dynamic transverse spin structure factor $S^{+-}(\mathbf{k}, \omega)$. Of course, at the two Abelian points, the C-C_0 reduce to the two gapless Goldstone modes. They should smoothly crossover to those in figure 2 achieved by the LSWE in the strong coupling regime shown in figure 7(b). Note that the weak Y-y state still respects the spin–orbital coupled $U(1)_{\mathrm{soc}}$ symmetry $[H_f, \sum_i (-1)^{i_x} c_i^\dagger \sigma^y c_i] = 0$. However, the mirror symmetry valid in the strong coupling limit does not hold anymore in the weak coupling limit. So there is a crossover from weak to strong coupling where all the physical quantities evolve from having $\mathcal{M}$ asymmetry to owning $\mathcal{M}$ symmetry with respect to $\beta = \pi/4$. The next order terms $\sim t^4/U^3$ in the strong coupling expansion which include a ring exchange term around a fundamental square and do not have such a mirror symmetry. They may be needed to describe the crossover in figure 8. The crossover driven by $U > 0$ is dual to the BCS to BEC crossover driven by $U < 0$ in SOC coupled Fermi systems discussed in [51].

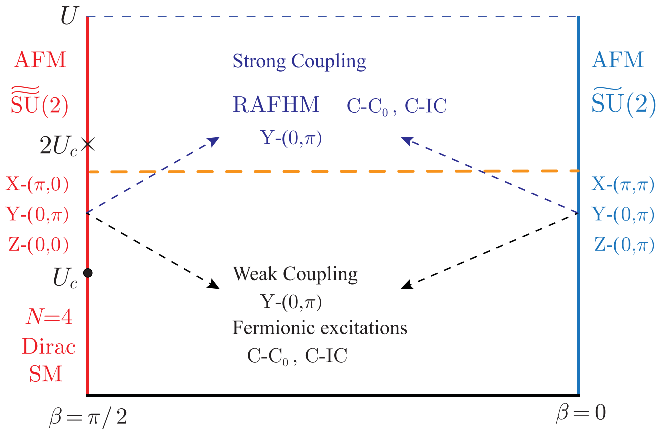

Figure 8. At any weak $U > 0$, the Y-y state emerges as the ground state at any non-Abelian point $0 < \beta < \pi/2$. At the Abelian point $\beta = 0$, any $U > 0$ leads to an antiferromagnetic state in the $\tilde{SU}(2)$ basis, three of which are listed on the $\beta = 0$ axis. At the Abelian point $\beta = \pi/2$ with the Abelian flux $\theta = \pi$, it is a semi-metal with $N = 4$ Dirac fermions, a finite critical U_c is needed to get to an antiferromagnetic state in the $\tilde{\tilde{SU}}(2)$ basis, three of which are also listed on the $\beta = \pi/2$ axis. One can see that only the Y-y state appears in both axes. At any point away from the two Abelian axes, it picks up the Y-y state as the ground state along the line (see also footnote 7) as indicated by the dashed line. There are both low energy fermionic excitations and C-C$_0$, C-IC relativistic magnon excitations in the weak coupling. However, there is no mirror symmetry anymore in the weak Y-y state. There is only a crossover from the weak to the strong coupling at any non-Abelian points.

7. High temperature expansions, electronic and spin Wilson loops at weak and strong coupling

In the classical fluctuation regime shown in figure 4, the Y-y state to the paramagnet transition in the RAFHM is in the same universality class as that from the Y-x state to the paramagnet transition in the RFHM in [25] which was shown to be in the 2D Ising universality class [49]. In the high temperature regime in figure 4, from the high temperature expansions in the $T_c \sim J \ll T \ll U$ limit, one can easily establish the relation between the free energy of RAFHM and that of the RFHM in [25]:

$$F^H_{\mathrm{RAFHM}}[J] = F^H_{\mathrm{RFHM}}[-J]. \tag{16}$$

Of course, the above relation breaks down in the symmetry breaking low temperature phases. Taking equation 18 in [25] and changing J to $-J$ leads to a high temperature expansion of the RAFHM:

$$C_m/N = \frac{3}{8}\left(\frac{J}{T}\right)^2 + \frac{3}{16}\left(\frac{J}{T}\right)^3 + \frac{6W_R - 39}{128}\left(\frac{J}{T}\right)^4 \tag{17}$$

where $W_R = 2\cos 4\beta + 1$ is the Wilson loop around the fundamental square given in section 2. The discussions below equation (18) in [25] also apply here.

In the weak coupling $U \ll t \ll T$ limit, following the method in [8], we perform the high temperature expansion in the limit $T \gg t$ directly on the fermionic model equation (1) to evaluate its specific heat:

$$C_f(T)/N = \frac{4t^2}{T^2} - (16 + 2W_f)\frac{t^4}{T^4} + \cdots \tag{18}$$

which establishes its connection with the electronic Wilson loops W_f given in section 1. Note that equation (1) is invariant under $t \to -t$, so there is no odd power of the t/T term in the expansion, in contrast to equation (17) which has odd power of terms. The term in the $(t/T)^4$ power proportional to the electronic Wilson loop W_f comes from the fermion hopping around a closed plaquette in the square lattice. Because $U \ll t$, the interaction effects may be dropped in equation (18), so it is essentially a free fermion hopping in a non-Abelain gauge potential. And so the crossover driven by the interaction U at the low temperature Y-y state in figure 7 can also be partially seen by looking at the specific heat crossover from equation (18) to equation (17) in the high temperature paramagnet state.

8. Experimental realizations and detections

In condensed matter systems, as said in the introduction, any of the linear superpositions of the Rashba SOC $k_x\sigma_x + k_y\sigma_y$ and Dresselhaus SOC $k_x\sigma_x - k_y\sigma_y$ always exist in various noncentrosymmetric 2D or layered materials. In momentum space, such a linear combination $\alpha k_x\sigma_x + \beta k_y\sigma_y$ can be written as the kinetic term in equation (1) in a periodic array of adsorbed ions with the SOC parameter (α, β) where the anisotropy can be adjusted by the strains, the shape of the surface or gate electric fields. The interaction strength U in equation (1) ranges from weak to strong in different materials [13, 14]. So all the phenomena in figure 8 can be observed in these materials.

In cold atom systems, in view of recent experimental advances to realize 2D Rashba or Dresselhaus SOC [17, 20], both the original and the $U(1)$ basis can be realized. Both gauge-invariant and non gauge-invariant quantities can be measured [31]. The gauge invariant quantities such as specific heat C_m [35, 36], the gaps Δ and the DOS [37], and the Wilson ratio can be detected by the corresponding experimental tools. The magnetization $M_Q(T)$, and the $(\pi,\ 0)$ and $(0,\ \pi)$ susceptibilities can be detected by the longitudinal atom or light Bragg spectroscopies [33, 34]. In the $U(1)$ basis in figure 1(b), one needs to measure the transverse structure factor at the four different ordering wavevectors $\mathbf{Q}_u=(0,\ 0)$, $\mathbf{Q}_x=(\pi,\ 0)$, $\mathbf{Q}_y=(0,\ \pi)$, $\mathbf{Q}_s=(\pi,\ \pi)$ in equation (10) by the transverse atom or light Bragg spectroscopies [33, 34] to get the whole transverse structure equation (11) in the EBZ. Before reaching $T<T_c\sim J$, the specific heat measurement [35, 36] at high temperatures to determine the whole set of fermionic or magnetic Wilson loops order by order in t/T equation (18) or J/T equation (17) could be performed easily. However, so far, the interaction in these cold atom experiments is still in the weak coupling limit. So the weak Y-y state, and both its fermionic and magnon excitations in figure 8 can still be observed by various detection methods [32–36] in the current available weak coupling limit. Because there is only a crossover from weak to strong coupling, the results on magnons achieved in the strong coupling limit still hold qualitatively in the weak coupling limit. When the heating issue is completely overcome as the interaction strength is tuned to the strong coupling limit, the RAFHM equation (2) can be realized and all the strong coupling results achieved here can be detected quantitatively.

9. Discussions and conclusions

There are previous theoretical works to study strongly correlated spinless bosons in Abelian gauge fields [40–44] and spinor bosons in non-Abelian gauge fields [25, 45–49]. The topological quantum phase transitions of non-interacting fermions driven by a Rashba type of SOC are investigated in a honeycomb lattice [31]. Various itinerant phases and phase transitions of repulsively interacting fermions subject to Weyl type SOC in a 3D continuum were studied in [50]. The BCS to BEC crossover of attractively interacting fermions tuned by the strengths of various forms of SOC in 2D and 3D continua were explored in [51]. However, so far, there are very few works to study the possible dramatic effects of SOC on strongly correlated electron systems on lattice systems. In this paper, we investigate the system of interacting fermions at half filling hopping in a 2D square lattice subject to any combinations of Rashba and Dresselhaus SOC described by equation (1). In the strong coupling limit, we reach a novel quantum spin model, the RAFHM (equation (2)), which is a new class of quantum spin model. Along the anisotropic line $(\alpha=\pi/2,\ \beta)$, its ground state is a new kind of spin and bond correlated magnetic state called the Y-y state in figure 1(a) which supports a novel excitation called C-IC magnons in a large SOC parameter regime $\beta_1<\beta<\beta_2$ in figure 2(a).

The C-IC magnons in the RAFHM stand for the short-ranged IC seeds embedded in a commensurate long-range ordered Y-y state. Their parameters such as the minimum positions $(0,\ k_y^0)$, gap and velocities v_x, v_y can be precisely measured by the peak positions, width and Lorentzian shape of the transverse structure factor at $T=0$, respectively. In this sense, they resemble quite closely an elementary particle resonance in scattering cross sections in particle physics. It remains interesting to see how these seeds respond under various external probes. To transfer the short-ranged IC order to a long-ranged one, one needs to apply an external probe to drag it out and then drive its condensation. We will study how these magnons respond under a finite $(\pi,\ 0)$ longitudinal field h_y which couples to the conserved quantity and still keeps the spin–orbital coupled $U(1)$ symmetry or two different $(\pi,\ 0)$ transverse fields h_x and h_z which breaks it explicitly.

It may be necessary to point out the RAFHM equation (2) is explicit for spin $S=1/2$. However, the RFHM in [25, 26, 48, 49] is for any spin $S=N/2$. As argued in [48], the critical temperature $T_c/J\sim 2S$, so increasing the spin is a very effective way to raise the critical temperature. It is known that if putting $S=3/2$ fermions on a lattice without SOC, the resulting spin model in the strong coupling limit at half filling [52] has a higher symmetry such as $SO(5)$ instead of $SU(2)$, and it has even larger quantum fluctuations due to the enlarged symmetry. It remains important to achieve any spin-S RAFHM.

As mentioned in the introduction, starting from the results achieved in this paper along the solvable line $(\alpha=\pi/2,\ \beta)$, we will investigate the quantum or topological phenomena at a generic equivalent class $(\alpha,\ \beta)$ including the isotropic Rashba or Dresselhauss lines $\alpha=\pm\beta$ at both the weak and strong coupling limit. Recently, the same 'divide and conquer' approach has been employed to map out the very rich and novel phenomena of RFHM in the generic SOC parameter $(\alpha,\ \beta)$ in [26]. As shown in this paper, the RAFHM displays quite different phenomena than those in the RFHM [25] along the solvable line $(\alpha=\pi/2,\ \beta)$. So we expect that the global phase diagram of RAFHM equation (2) may also show quite different phenomena than those of RFHM in [26]. Expansion to the t^3/U^2 order which includes ring exchange terms around a square plaquette may also be necessary to study the possible phases and phase transitions from the weak to strong coupling limit. The SOC could provide a new mechanism to lead to spin liquid phases with topological orders even in a bipartite lattice. Possible topological spin liquid phases in a honeycomb lattice with three SOC parameters (α, β, γ) need to be explored.

Acknowledgments

We acknowledge AFOSR FA9550-16-1-0412 for their support. WML is supported by the NKRDP under grant nos. 2016YFA0301500, NSFC under grant nos. 11434015, 61227902, 61378017, SKLQOQOD under grant nos. KF201403 and SPRPCAS under grant nos. XDB01020300, XDB21030300.

Appendix

In this appendix, we provide some technical details on the results achieved in the main text. (1) The symmetry and symmetry breaking analysis of the fermionic and the RAFHM, followed by a specific linear spin wave expansion (LSWE) at $1/S$ order. (2) The $1/S$ correction to the LSWE results. (3) The structure of the quantum Y-y ground state which encodes the C-IC magnons. (4) The fermionic excitations in the Y-y state at weak coupling $U \ll t$.

Appendix A. The linear spin wave expansion

Here we present the specific spin wave calculations which can be contrasted with the exact statements made in section 2. After introducing two HP bosons a, b corresponding to the two sublattices A, B in figure 1(a), we obtain the Hamiltonian at the LSWE $1/S$ order:

$$\mathcal{H}_2 = 2\sum_{\mathbf{k}}(a_{\mathbf{k}}^{\dagger}a_{\mathbf{k}} + b_{\mathbf{k}}^{\dagger}b_{\mathbf{k}}) + \frac{1}{2}\sum_{\mathbf{k}}[\cos k_x(a_{-\mathbf{k}}a_{\mathbf{k}} + b_{-\mathbf{k}}b_{\mathbf{k}}) + \cos(k_y + 2\beta)a_{-\mathbf{k}}b_{\mathbf{k}} + \cos(k_y - 2\beta)b_{-\mathbf{k}}a_{\mathbf{k}} + \text{h.c.}]. \tag{A.1}$$

We first perform a unitary transformation:

$$\begin{pmatrix} a_{\mathbf{k}} \\ b_{\mathbf{k}} \end{pmatrix} = U_{\mathbf{k}}\begin{pmatrix} \bar{a}_{\mathbf{k}} \\ \bar{b}_{\mathbf{k}} \end{pmatrix}, \quad U_{\mathbf{k}} = \begin{pmatrix} \sin\frac{\theta_{\mathbf{k}}}{2} & \cos\frac{\theta_{\mathbf{k}}}{2} \\ -\cos\frac{\theta_{\mathbf{k}}}{2} & \sin\frac{\theta_{\mathbf{k}}}{2} \end{pmatrix} \tag{A.2}$$

where $\sin\theta_k = \frac{\cos k_x}{\sqrt{\cos^2 k_x + \sin^2 2\beta \sin^2 k_y}}$, $\cos\theta_k = \frac{\sin 2\beta \sin k_y}{\sqrt{\cos^2 k_x + \sin^2 2\beta \sin^2 k_y}}$ is identical to that used in the RFHM [25] to cast the Hamiltonian equation (A.1) into a simple form:

$$\mathcal{H}_2 = \sum_k \begin{pmatrix} \bar{a}_k^{\dagger} \\ \bar{a}_{-k} \end{pmatrix}^{\top} \begin{pmatrix} 1 & \lambda_k^- \\ \lambda_k^- & 1 \end{pmatrix} \begin{pmatrix} \bar{a}_k \\ \bar{a}_{-k}^{\dagger} \end{pmatrix} + \sum_k \begin{pmatrix} \bar{b}_k^{\dagger} \\ \bar{b}_{-k} \end{pmatrix}^{\top} \begin{pmatrix} 1 & \lambda_k^+ \\ \lambda_k^+ & 1 \end{pmatrix} \begin{pmatrix} \bar{b}_k \\ \bar{b}_{-k}^{\dagger} \end{pmatrix} \tag{A.3}$$

where $\lambda_k^{\pm} = \pm\text{sgn}(\cos k_x)\gamma_k^{\pm}$ and the $\gamma_k^{\pm} = \frac{1}{2}[\cos 2\beta \cos k_y \pm \sqrt{\cos^2 k_x + \sin^2 2\beta \sin^2 k_y}]$ which is also listed below equation (4).

Then we perform the Bogoliubov transformations:

$$\begin{pmatrix} \bar{a}_k \\ \bar{a}_{-k}^{\dagger} \end{pmatrix} = \begin{pmatrix} \cosh\phi_k^- & \sinh\phi_k^- \\ \sinh\phi_k^- & \cosh\phi_k^- \end{pmatrix} \begin{pmatrix} \alpha_k \\ \alpha_{-k}^{\dagger} \end{pmatrix}, \quad \begin{pmatrix} \bar{b}_k \\ \bar{b}_{-k}^{\dagger} \end{pmatrix} = \begin{pmatrix} \cosh\phi_k^+ & \sinh\phi_k^+ \\ \sinh\phi_k^+ & \cosh\phi_k^+ \end{pmatrix} \begin{pmatrix} \beta_k \\ \beta_{-k}^{\dagger} \end{pmatrix} \tag{A.4}$$

where $2\phi_{\mathbf{k}}^- = -\text{arcsinh}(\lambda_{\mathbf{k}}^-/\omega_{\mathbf{k}}^-)$, $2\phi_{\mathbf{k}}^+ = -\text{arcsinh}(\lambda_{\mathbf{k}}^+/\omega_{\mathbf{k}}^+)$ to transform the Hamiltonian equation (A.3) to the diagonal form equation (4):

$$\mathcal{H}_2 = \sum_{\mathbf{k}}(\omega_{\mathbf{k}}^- + \omega_{\mathbf{k}}^+ - 2) + 2\sum_{\mathbf{k}}(\omega_{\mathbf{k}}^-\alpha_{\mathbf{k}}^{\dagger}\alpha_{\mathbf{k}} + \omega_{\mathbf{k}}^+\beta_{\mathbf{k}}^{\dagger}\beta_{\mathbf{k}})$$

where $\omega_{\mathbf{k}}^{\pm} = \sqrt{1 - (\gamma_{\mathbf{k}}^{\pm})^2}$.

When $\beta < \pi/4$, $\omega_k^+ < \omega_k^-$, when $\beta > \pi/4$, $\omega_k^+ > \omega_k^-$, at $\beta = \pi/4$, $\omega_k^+ = \omega_k^-$. In the main text, for notational simplicity, we assume ω_k^- is always the lower branch. The minima of the excitation spectrum $\mathbf{k}^0 = (0, k_y^0)$ can be determined as:

$$k_y^0(\beta) = \begin{cases} 0, & 0 < \beta < \beta_1 \\ \pm\arccos[\sqrt{1 + \sin^2 2\beta}/\tan 2\beta], & \beta_1 < \beta < \pi/4 \end{cases} \tag{A.5}$$

where $k_y^0(\beta) = k_y^0(\pi/2 - \beta)$, $\pi/4 < \beta < \pi/2$ which is shown in figure 2(a). Note that the β_1 and β_2 coincide with those in RFHM [25].

Expanding around the minima leads to the relativistic form equation (5) where the mass and the two velocities are given by:

$$\Delta^2 = 1 - (1 + \cos 2\beta)^2/4, \quad v_x^2 = \cos^2\beta/2, \quad v_y^2 = \cos^2\beta(\cos^2 2\beta + \cos 2\beta - 1)/2, \quad 0 < \beta < \beta_1, \tag{A.6}$$

$$\Delta^2 = (3 - \csc^2 2\beta)/4, \quad v_x^2 = 1/(4\sin^2 2\beta), \quad v_y^2 = (\sin^4 2\beta + \sin^2 2\beta - 1)/(4\sin^4 2\beta), \quad \beta_1 < \beta < \pi/4 \tag{A.7}$$

which are shown in figure 2(b). It is easy to check that as $\beta \to 0$, $\Delta \sim \sqrt{2}\beta \to 0$, $v_x \to 1/\sqrt{2}$, $v_y \to 1/\sqrt{2}$. So the dispersion $\omega_q \to v|\mathbf{q}|$ is as it should be. Note that the QC regime in figure 4 is defined as $\beta \ll T$.

The dispersion relations of both C-C$_0$ and C-IC take the relativistic form with the mass Δ and two velocities v_x and v_y. The anisotropy between the two velocities at $\beta \neq \pi/4$ is irrelevant under the renormalization group (RG), so the relativistic invariance is restored under the RG. In sharp contrast, all the magnons in the RFHM [25] are non-relativistic gapped particles with a gap Δ and two effective masses $m_y \geqslant m_x$. Note that it is the Bogoliubov transformation equation (A.4) which leads to quantum fluctuations at $T = 0$ and makes the RAFHM dramatically different from the RFHM [25].

Appendix B. 1/S corrections to the linear spin wave results

Normal-ordering $\mathcal{H}_4$ in the quasi-particle α, β basis in equation (4) (namely with respect to the quantum ground state $|\Omega\rangle$ in the next section) results in the three terms:

$$\mathcal{H}_4 = \mathcal{H}_4^{(0)} + \mathcal{H}_4^{(2)} + \mathcal{H}_4^{(4)} \tag{B.1}$$

where $\mathcal{H}_4^{(0)}$ is a constant term, $\mathcal{H}_4^{(2)}$ is quadratic and $\mathcal{H}_4^{(4)}$ is quartic in terms of α, β. Following [29], it is easy to see that $\mathcal{H}_4^{(0)}$ and $\mathcal{H}_4^{(2)}$ contribute to the ground state energy and energy spectrum at the order of $1/S$ corrections to the LSWE respectively. While $\mathcal{H}_4^{(4)}$ only make contributions at a higher order than $1/S^2$, so can be dropped at the order of $1/S$.

The $\mathcal{H}_4^{(0)}$ leads to the $1/S$ corrections (in unit $2JS$) to the ground state energy listed in equation (6):

$$\mathcal{H}_4^{(0)} = -\frac{N}{8S}[I_0^2 + I_c^2 + I_s^2] \tag{B.2}$$

where,

$$\begin{aligned}
I_0(\beta) &= \int \frac{\mathrm{d}^2k}{4\pi^2}\left[\cos k_x \sin\theta_k\left(\frac{\gamma_k^-}{\omega_k^-} - \frac{\gamma_k^+}{\omega_k^+}\right) + \frac{1}{\omega_k^-} + \frac{1}{\omega_k^+} - 2\right],\\
I_c(\beta) &= \int \frac{\mathrm{d}^2k}{4\pi^2}\left[-\cos k_y\left(\frac{\gamma_k^-}{\omega_k^-} + \frac{\gamma_k^+}{\omega_k^+}\right) + \left(\frac{1}{\omega_k^-} + \frac{1}{\omega_k^+} - 2\right)\cos 2\beta\right],\\
I_s(\beta) &= \int \frac{\mathrm{d}^2k}{4\pi^2}\left[\sin k_y \cos\theta_k\left(\frac{\gamma_k^-}{\omega_k^-} - \frac{\gamma_k^+}{\omega_k^+}\right) + \left(\frac{1}{\omega_k^-} + \frac{1}{\omega_k^+} - 2\right)\sin 2\beta\right].
\end{aligned} \tag{B.3}$$

The numerical result of equation (B.2) for $S = 1/2$ was drawn in figure 3(a). There is always a $1/S$ correction to the ground state energy shown in figure 3(a), but this is found to be small.

The $\mathcal{H}_4^{(2)}$ can be written as in the normal ordered form:

$$\begin{aligned}
\mathcal{H}_4^{(2)} = &-\frac{1}{4S}\sum[2(I_0 + I_c\cos 2\beta + I_s\sin 2\beta)(A_k^\dagger A_k + A_k^\dagger C_{-k}^\dagger + B_k^\dagger B_k + B_k^\dagger D_{-k}^\dagger + \mathrm{h.c.})\\
&+ 2I_0\cos k_x(A_{-k}A_k + C_{-k}^\dagger A_{-k} + C_k^\dagger A_k + C_k^\dagger C_{-k}^\dagger + B_{-k}B_k + D_{-k}^\dagger B_{-k} + D_k^\dagger B_k + D_k^\dagger D_{-k}^\dagger + \mathrm{h.c.})\\
&+ 2(I_c\cos k_y - I_s\sin k_y)(A_{-k}B_k + D_{-k}^\dagger A_{-k} + C_k^\dagger B_k + C_k^\dagger D_{-k}^\dagger + \mathrm{h.c.})]
\end{aligned} \tag{B.4}$$

where A, B, C, D are the annihilation operators in terms of α, β:

$$\begin{aligned}
A_k &= \sin(\theta_k/2)\cosh\phi_k^-\alpha_k + \cos(\theta_k/2)\cosh\phi_k^+\beta_k,\\
B_k &= -\cos(\theta_k/2)\cosh\phi_k^-\alpha_k + \sin(\theta_k/2)\cosh\phi_k^+\beta_k\\
C_{-k} &= \sin(\theta_k/2)\sinh\phi_k^-\alpha_{-k} + \cos(\theta_k/2)\sinh\phi_k^+\beta_{-k},\\
D_{-k} &= -\cos(\theta_k/2)\sinh\phi_k^-\alpha_{-k} + \sin(\theta_k/2)\sinh\phi_k^+\beta_{-k}.
\end{aligned}$$

Following [29], it is straightforward to evaluate the $1/S$ correction the spectrum equation (4) obtained at the LSWE, which, in turn, changes the gap and leads to the shifts of β_1, β_2, the minimum positions $(0,\ k_y^0)$ of the C-IC relativistic magnons as shown in figure 2. We also evaluate its contribution to the magnetization shown in figure 3(b). They are all at $\beta = \pi/4$, in a suitably chosen rotated basis, we find $\mathcal{H}_4^{(2)}$ can be written as $\mathcal{H}_4^{(2)} = C'\sum_{\mathbf{k}}(\omega_{\mathbf{k}}^{-}\alpha_{\mathbf{k}}^{\dagger}\alpha_{\mathbf{k}} + \omega_{\mathbf{k}}^{+}\beta_{\mathbf{k}}^{\dagger}\beta_{\mathbf{k}})$ which just contributes a multiple factor C' to the LSWE spectrum in equation (4), so it does not change the magnetization in figure 3(b) at the order of $1/S$. There is no $1/S$ correction to the magnetization at the two Abelian points $\beta = 0,\ \pi/2$, consistent with the results achieved for the antiferromagnetic Heisenberg model [29]. Of course, it does not shift the minima positions $(0,\ k_y^0 = \pm\pi/2)$ in figure 2(a) as dictated by the mirror symmetry. It does lead to a multiple factor to the gap at the order of $1/S$ shown in figure 2(b). There are $1/S$ corrections at any other β shown in figure 3(b), but found to be small even at $S = 1/2$. We expect that the magnetization will receive $1/S^2$ corrections at $\beta = 0,\ \pi$ as calculated in [29] and also at $\beta = \pi/4$.

Note that $(\beta_1,\ \beta_2)$ in figure 2(a) takes the same values as those in the RFHM at the order $1/S$. This is because, as shown in the last section, the two models share the same unitary transformation equation (A.2). However, the main difference is that the RAFHM also involves a Bogoliubov transformation equation (A.4) which induces quantum fluctuations at $T = 0$. In sharp contrast, the Y-x ground state is exact for the RFHM [25], there are no quantum corrections to any orders in $1/S$ at $T = 0$. So in the RFHM, β_1 is exact, and will not receive any quantum corrections from higher order expansions in $1/S$. While, in the RAFHM, β_1 is not exact, and does receive quantum corrections from higher order expansions in $1/S$. The contributions at the $1/S$ order are shown in figure 2(a) and found to be very small.

Note that the mirror symmetry dictates that (1) the minima positions in figure 2(a) are exactly symmetric about $\beta = \pi/4$; (2) the minimum position at $\beta = \pi/4$ is exactly pinned at $(0,\ k_y^0 = \pi/2)$; and (3) the relation $\beta_2 = \pi/2 - \beta_1$ is exact. All these three exact statements should receive no corrections to any orders in $1/S$. Indeed, we find they receive no correction at the $1/S$ order.

Appendix C. Quantum corrections to the classical state and the $U(1)_{\mathrm{SOC}}$ symmetry of the quantum ground state to the order $1/S$

C.1. Quantum corrections to the classical Y-y state

The Y-x state is the exact ground state of the RHFM [25], so there are no quantum fluctuations. However, the Y-y state in figure 1(a) is only classical, valid only at $S = \infty$. Any finite S causes quantum corrections to the classical ground state. The quantum corrections to Halperin's $(1,\ 1,\ 1)$ state in the bilayer or trilayer quantum Hall state due to the neutral gapless Goldstone mode were investigated in [38, 39]. In fact, the $(1,\ 1,\ 1)$ state is a ferromagnetic state which is exact only when distance between the two layers vanishes. At any finite distance, it suffers quantum fluctuations and should receive quantum corrections. Similar quantum corrections to the classical Bose–Einstein condensation (BEC) $\langle\Psi\rangle = a \neq 0$ in superfluid helium can also be evaluated.

Using the fact that $|\Omega\rangle$ is the vacuum of the quasi-particle operators: $\alpha_k|\Omega\rangle = \beta_k|\Omega\rangle = 0$, we find the quantum fluctuations corrected ground state at the order $1/S$:

$$|\Omega\rangle = \mathcal{C}\exp\left\{\sum_k\left[\sin\theta_k\left(\frac{1-\omega_k^-}{2\gamma_k^-} + \frac{\omega_k^+ - 1}{2\gamma_k^+}\right)(a_k^\dagger a_{-k}^\dagger + b_k^\dagger b_{-k}^\dagger) + 2\sin^2\left(\frac{\theta_k}{2}\right)\left(\frac{\omega_k^- - 1}{\gamma_k^-} + \frac{\omega_k^+ - 1}{\gamma_k^+}\right)a_k^\dagger b_{-k}^\dagger\right]\right\}|\text{Y-y}\rangle \tag{C.1}$$

which establishes the connection between the quantum ground state $|\Omega\rangle$ and the classical ground state $|\text{Y-y}\rangle$. Obviously, $|\text{Y-y}\rangle$ is the vacuum of the original boson operators a and b, while $|\Omega\rangle$ is that of the quasi-particle operators α_k and β_k which contain all the information of the quantum fluctuation generated C-C$_0$ and C-IC magnons.

C.2. The $U(1)_{\mathrm{SOC}}$ symmetry of the quantum ground state

In the classical limit, we know $Q_c|\text{Y-y}\rangle = 0$ where $Q_c = \sum_i(-1)^{i_x}S_i^y$ is the conserved quantity along the line. Here we show that in the strong coupling limit, the quantum fluctuations corrected ground state $|\Omega\rangle$ also satisfies $Q_c|\Omega\rangle = 0$ at the order $1/S$.

For notational convenience, we apply a global rotation $(S_i^x,\ S_i^y,\ S_i^z) \to (\tilde{S}_i^x,\ \tilde{S}_i^z,\ -\tilde{S}_i^y)$ to rotate S^y to $\tilde{S}_i^z$, then the conserved quantity takes the form:

$$Q_c = \sum_i(-1)^{i_x}S_i^y = \sum_i(-1)^{i_x}\tilde{S}_i^z = -\sum_k(a_k^\dagger a_{k+Q_x} - b_k^\dagger b_{k+Q_x}) \tag{C.2}$$

where $Q_x = (\pi,\ 0)$ is the orbital structure of conserved quantity Q_c.

Combining equation (A.2) and equation (A.4) leads to:

$$
\begin{aligned}
a_k^\dagger &= \sin(\theta_k/2)\bar{a}_k^\dagger + \cos(\theta_k/2)\bar{b}_k^\dagger = \sin(\theta_k/2)(u_k^a\alpha_k^\dagger + v_k^a\alpha_{-k}) + \cos(\theta_k/2)(u_k^b\beta_k^\dagger + v_k^b\beta_{-k})\\
b_k^\dagger &= \sin(\theta_k/2)\bar{b}_k^\dagger - \cos(\theta_k/2)\bar{a}_k^\dagger = \sin(\theta_k/2)(u_k^b\beta_k^\dagger + v_k^b\beta_{-k}) - \cos(\theta_k/2)(u_k^a\alpha_k^\dagger + v_k^a\alpha_{-k}).
\end{aligned} \tag{C.3}
$$

Using $\alpha_k|\Omega\rangle = \beta_k|\Omega\rangle = 0$ and the bosonic commutation relations of α_k, β_k simplifies it to:

$$
\begin{aligned}
a_k^\dagger a_{k+Q_x}|\Omega\rangle = {}&[\sin(\theta_k/2)u_k^a\alpha_k^\dagger + \cos(\theta_k/2)u_k^b\beta_k^\dagger][\sin(\theta_{k+Q_x}/2)v_{k+Q_x}^a\alpha_{-k-Q_x}^\dagger\\
&+ \cos(\theta_{k+Q_x}/2)v_{k+Q_x}^b\beta_{-k-Q_x}^\dagger]|\Omega\rangle\\
b_k^\dagger b_{k+Q_x}|\Omega\rangle = {}&[\sin(\theta_k/2)u_k^b\beta_k^\dagger - \cos(\theta_k/2)u_k^a\alpha_k^\dagger][\sin(\theta_{k+Q_x}/2)v_{k+Q_x}^b\beta_{-k-Q_x}^\dagger\\
&- \cos(\theta_{k+Q_x}/2)v_{k+Q_x}^a\alpha_{-k-Q_x}^\dagger]|\Omega\rangle
\end{aligned} \tag{C.4}
$$

thus,

$$
\begin{aligned}
Q_c|\Omega\rangle = {}&\sum_k(\cos[(\theta_k + \theta_{k+Q_x})/2]u_k^a v_{k+Q_x}^a\alpha_k^\dagger\alpha_{-k-Q_x}^\dagger - \cos[(\theta_k + \theta_{k+Q_x})/2]u_k^b v_{k+Q_x}^b\beta_k^\dagger\beta_{-k-Q_x}^\dagger\\
&- \sin[(\theta_k + \theta_{k+Q_x})/2]u_k^a v_{k+Q_x}^b\alpha_k^\dagger\beta_{-k-Q_x}^\dagger - \sin[(\theta_k + \theta_{k+Q_x})/2]v_{k+Q_x}^a u_k^b\alpha_{-k-Q_x}^\dagger\beta_k^\dagger)|\Omega\rangle.
\end{aligned} \tag{C.5}
$$

From equation (A.2), one can see $\theta_k + \theta_{k+Q_x} = 0$, so the above equation is simplified to:

$$
\begin{aligned}
Q_c|\Omega\rangle &= \sum_k u_k^a v_{k+Q_x}^a\alpha_k^\dagger\alpha_{-k-Q_x}^\dagger|\Omega\rangle - \sum_k u_k^b v_{k+Q_x}^b\beta_k^\dagger\beta_{-k-Q_x}^\dagger|\Omega\rangle\\
&= \sum_k\frac{1}{2}(u_k^a v_{k+Q_x}^a + u_{k+Q_x}^a v_k^a)\alpha_k^\dagger\alpha_{-k-Q_x}^\dagger|\Omega\rangle - \sum_k\frac{1}{2}(u_k^b v_{k+Q_x}^b + u_{k+Q_x}^b v_k^b)\beta_k^\dagger\beta_{-k-Q_x}^\dagger|\Omega\rangle.
\end{aligned} \tag{C.6}
$$

From equation (A.4), one can see $\lambda_{k+Q_x}^\pm = -\lambda_k^\pm$ and $\omega_{k+Q_x}^\pm = \omega_k^\pm$, which leads to $Q_c|\Omega\rangle = 0$ at the order of $1/S$. Of course, it should hold exactly, so to any order of $1/S$.

Although the classical Y-y state contains no information on the C-C_0, C-IC relativistic magnons, the quantum ground state $|\Omega\rangle$ does contain it and can be detected by the transverse structure factor equation (11) precisely.

Appendix D. The fermionic excitations in the Y-y state at weak coupling $U \ll t$

The two branches of gapped fermionic excitations in the Y-y state at weak coupling are:

$$
\begin{aligned}
\epsilon_1 &= 2t\sqrt{\sin^2 k_x + \cos^2\beta\cos^2 k_y + \sin^2\beta\sin^2 k_y + \frac{M^2}{16t^2} - 2\sqrt{\cos^2\beta\cos^2 k_y(\sin^2 k_x + \sin^2\beta\sin^2 k_y)}}\\
\epsilon_2 &= 2t\sqrt{\sin^2 k_x + \cos^2\beta\cos^2 k_y + \sin^2\beta\sin^2 k_y + \frac{M^2}{16t^2} + 2\sqrt{\cos^2\beta\cos^2 k_y(\sin^2 k_x + \sin^2\beta\sin^2 k_y)}}
\end{aligned} \tag{D.1}
$$

where $M \sim e^{-3/[4U\rho_0(\beta)]}$ where $\rho_0(\beta)$ is the DOS at the FS in figure 7(a) with the asymptotic behavior $\rho_0(\beta) \sim \ln 1/\beta$ when $\beta \to 0$ and $\rho_0(\beta) \to 0$ when $\beta \to \pi/2^-$.

References

[1] Schrieffer J R, Wen X G and Zhang S C 1989 Dynamic spin fluctuations and the bag mechanism of high-T, superconductivity *Phys. Rev.* B **39** 11663

[2] Chubukov A V, Sachdev S and Ye J 1994 Theory of two-dimensional quantum Heisenberg antiferromagnets with a nearly critical ground state *Phys. Rev.* B **49** 11919

[3] Auerbach A 1994 *Interacting Electrons and Quantum Magnetism* (Berlin: Springer)

[4] Wen X G 2004 *Quantum Field Theory of Many-Body Systems: From the Origin of Sound to an Origin of Light and Electrons* (Oxford: Oxford University Press)

[5] Sachdev S 2011 *Quantum Phase Transitions* 2nd edn (Cambridge: Cambridge University Press)

[6] Kivelson S A *et al* 2003 How to detect fluctuating stripes in the high-temperature superconductors *Rev. Mod. Phys.* **75** 1201

[7] Bychkov Y A and Rashba E I 1984 Oscillatory effects and the magnetic susceptibility of carriers in inversion layers *J. Phys.* C **17** 6039

[8] Ye J, Kim Y B, Millis A J, Shraiman B I, Majumdar P and Tesanovic Z 1999 Berry phase theory of the anomalous Hall effect: application to colossal magnetoresistance manganites *Phys. Rev. Lett.* **83** 3737

[9] Gor'kov L P and Rashba E I 2001 Superconducting 2D system with lifted spin degeneracy: mixed singlet-triplet state *Phys. Rev. Lett.* **87** 037004

[10] Jungwirth T, Niu Q and MacDonald A H 2004 Anomalous Hall effect in ferromagnetic semiconductors *Phys. Rev. Lett.* **88** 207208

[11] Sinova J *et al* 2004 Universal intrinsic spin Hall effect *Phys. Rev. Lett.* **92** 126603

[12] Yao W and Niu Q 2008 Berry phase effect on the exciton transport and on the exciton Bose–Einstein condensate *Phys. Rev. Lett.* **101** 106401

[13] Nagaosa N, Sinova J, Onoda S, MacDonald A H and Ong N P 2010 Anomalous Hall effect *Rev. Mod. Phys.* **82** 1539

[14] Sinova J, Valenzuela S O, Wunderlich J, Back C H and Jungwirth T 2015 Spin Hall effects *Rev. Mod. Phys.* **87** 1213
[15] Bloch I, Dalibard J and Zwerger W 2008 Many-body physics with ultracold gases *Rev. Mod. Phys.* **80** 885
[16] Hart R A *et al* 2015 Observation of antiferromagnetic correlations in the Hubbard model with ultracold atoms *Nature* **519** 211C214
[17] Huang L *et al* 2016 Experimental realization of a two-dimensional synthetic spin–orbit coupling in ultracold Fermi gases *Nat. Phys.* **12** 540–4
[18] Meng Z *et al* 2016 Experimental observation of a topological band gap opening in ultracold fermi gases with two-dimensional spin-orbit coupling *Phys. Rev. Lett* **117** 235304
[19] Wall M L *et al* 2016 Synthetic spin–orbit coupling in an optical lattice clock *Phys. Rev. Lett.* **116** 035301
[20] Wu Z *et al* 2016 Realization of two-dimensional spin–orbit coupling for Bose–Einstein condensates *Science* **354** 83–8
[21] Ye J 1996 Emery–Kivelson line and universality of Wilson ratio of spin anisotropic Kondo model *Phys. Rev. Lett.* **77** 3224
[22] Ye Jinwu 1997 Abelian bosonization approach to quantum impurity problems *Phys. Rev. Lett.* **79** 1385
[23] Rokhsar D S and Kivelson S A 1988 Superconductivity and the quantum hard-core dimer gas *Phys. Rev. Lett.* **61** 2376
[24] Yao H and Kivelson S A 2012 Exact spin liquid ground states of the quantum dimer model on the square and honeycomb lattices *Phys. Rev. Lett.* **108** 247206
[25] Sun F, Ye J and Liu W-M 2015 Quantum magnetism of spinor bosons in optical lattices with synthetic non-Abelian gauge fields *Phys. Rev.* A **92** 043609
[26] Sun F, Ye J and Liu W-M 2017 In-commensurate Skyrmion crystals, devil staircases and multi-fractals due to spin orbit coupling in a lattice system arXiv:1603.00451
[27] Scalettar R T, Batrouni G G, Kampf A P and Zimanyi G T 1995 Simultaneous diagonal and off-diagonal order in the Bose–Hubbard Hamiltonian *Phys. Rev.* B **51** 8467
[28] Murthy G, Arovas D and Auerbach A 1997 Superfluids and supersolids on frustrated two-dimensional lattices *Phys. Rev.* B **55** 3104
[29] Igarashi J-i 1992 1/S expansion for thermodynamic quantities in a two-dimensional Heisenberg antiferromagnet at zero temperature *Phys. Rev.* B **46** 10763
Igarashi J-i and Nagao T 2005 1MS-expansion study of spin waves in a two-dimensional Heisenberg antiferromagnet *Phys. Rev.* B **72** 014403
[30] Yu Y-X, Ye J and Liu W M 2013 Goldstone and Higgs modes of photons inside a cavity and their detections *Sci. Rep.* **3** 3476
[31] Sun F, Yu X-L, Ye J, Fan H and Liu W-M 2013 Topological quantum phase transition in synthetic non-Abelian gauge potential: gauge invariance and experimental detections *Sci. Rep.* **3** 2119
[32] Stewart J T, Gaebler J P and Jin D S 2008 Using photoemission spectroscopy to probe a strongly interacting Fermi gas *Nature* **454** 744
[33] Ye J *et al* 2011 Light-scattering detection of quantum phases of ultracold atoms in optical lattices *Phys. Rev.* A **83** 051604
[34] Ye J, Zhang K Y, Li Y, Chen Y and Zhang W P 2013 Optical Bragg, atom Bragg and cavity QED detections of quantum phases and excitation spectra of ultracold atoms in bipartite and frustrated optical lattices *Ann. Phys* **328** 103
[35] Kinast J *et al* 2005 Heat capacity of a strongly interacting Fermi gas *Science* **307** 1296
[36] Ku M J H *et al* 2012 Revealing the superfluid lambda transition in the universal thermodynamics of a unitary Fermi gas *Science* **335** 563
[37] Gemelke N, Zhang X, Huang C L and Chin C 2009 *In situ* observation of incompressible Mott-insulating domains in ultracold atomic gases *Nature (London)* **460** 995
[38] Jiang L and Ye J 2006 Ground state, quasihole and a pair of quasihole wavefunctions in bi-layer quantum Hall systems *Phys. Rev.* B **74** 245311
[39] Ye J 2005 Broken symmetry, excitons, gapless modes, and topological excitations in trilayer quantum Hall systems *Phys. Rev.* B **71** 125314
[40] Balents L, Bartosch L, Burkov A, Sachdev S and Sengupta K 2005 Putting competing orders in their place near the Mott transition *Phys. Rev.* B **71** 144508
[41] Jiang L and Ye J 2006 The mobility of dual vortices in honeycomb, square, triangular, Kagome and dice lattices *J. Phys.: Condens. Matter* **18** 6907
[42] Ye J 2008 Duality, magnetic space group and their applications to quantum phases and phase transitions on bipartite lattices in several experimental systems *Nucl. Phys.* B **805** 418
[43] Chen Y and Ye J 2012 Characterizing boson orders in lattices by vortex degree of freedoms *Phil. Mag.* **92** 4484–91
[44] Ye J and Chen Y 2013 Quantum phases, supersolids and quantum phase transitions of interacting bosons in frustrated lattices *Nucl. Phys.* B **869** 242
[45] Cai Z, Zhou X and Wu C 2012 Magnetic phases of bosons with synthetic spin–orbit coupling in optical lattices *Phys. Rev.* A **85** 061605(R)
[46] Radic J, Di Ciolo A, Sun K and Galitski V 2012 Exotic quantum spin models in spin–orbit-coupled Mott insulators *Phys. Rev. Lett.* **109** 085303
[47] Cole W S, Zhang S, Paramekanti A and Trivedi N 2012 Bose–Hubbard models with synthetic spin–orbit coupling: mott insulators, spin textures, and superfluidity *Phys. Rev. Lett.* **109** 085302
[48] Sun F, Ye J and Liu W-M 2015 Quantum incommensurate Skyrmion crystals and commensurate to in-commensurate transitions in cold atoms and materials with spin orbit couplings in a Zeeman field arXiv:1502.05338
[49] Sun F, Ye J and Liu W-M 2016 Classification of magnons in rotated ferromagnetic Heisenberg model and their competing responses in transverse fields *Phys. Rev.* B **94** 024409
[50] Zhang S-S, Ye J and Liu W-M 2016 Itinerant magnetic phases and quantum Lifshitz transitions in repulsively interacting spin–orbit coupled Fermi gas *Phys. Rev.* B **94** 115121
[51] Yu Y-X, Ye J and Liu W-M 2014 Coherence lengths in attractively interacting Fermi gases with spin–orbit coupling *Phys. Rev.* A **90** 053603
[52] Wu C, Hu J-P and Zhang S-C 2003 Exact SO(5) symmetry in the spin-3/2 fermionic system *Phys. Rev. Lett.* **91** 186402